Journal of Hydrology: Regional Studies 46 (2023) 101322

Contents lists available at ScienceDirect

Journal of Hydrology: Regional Studies

journal homepage: www.elsevier.com/locate/ejrh

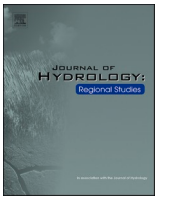

Streamflow trends of the Pyrenees using observations and multi-model approach (1980–2013)

Roger Clavera-Gispert [a,*], Pere Quintana-Seguí [a], Leticia Palazón [b], Ane Zabaleta [c], Omar Cenobio [a], Anaïs Barella-Ortiz [a], Santiago Beguería [b,*]

[a] Observatori de l'Ebre (Universitat Ramon Llull - CSIC), Roquetes, Spain
[b] Estación Experimental de Aula Dei (EEAD - CSIC), Zaragoza, Spain
[c] Zientzia eta Teknologia Fakultatea. Euskal Herriko Unibertsitatea UPV/EHU, Leioa, Spain

ARTICLE INFO

Keywords:
Pyrenees
Stream flow trends
Hydrological modeling
Climate variability
Land use
Land cover

ABSTRACT

Study region: The Pyrenees.
Study focus: The Pyrenees is sensitive to changes in climate (both natural and of anthropic origin) and changes in land use and cover (LULC). These changes can influence the water resources. The historical evolution (1980–2013) of the stream flows are studied using observed time series from non-influenced gauging stations and two models (SASER and SWAT). Their comparison helps to detect and analyze changes in flow rates and their trends (trends are computed using the Sen's slope estimator, the significance of which was evaluated using the Mann-Kendall test). Furthermore, it also allows to explore the question of attribution (these models do not simulate LULC change).
New hydrological insights for the region: A complex and diverse domain such as the Pyrenees gives large differences between modelled trends revealing a large uncertainty that has been observed thanks to the use of two models. For the study period, mostly there are no significant trends. When trends are present in the observations and are also simulated, they are attributed to the effects of climate (natural variability and human induced climate change). When the significant trends observed are not simulated by the models, they are mainly attributed to changes in LULC. In general, models have difficulties detecting observed trends, leading to their attribution to changes in LULCs rather than climate, but there are some notable exceptions.

1. Introduction

The Pyrenees, which extends from the Atlantic to the Mediterranean, is particularly sensitive to changes in climate (due to both natural variability and human induced climate change), as well as to changes in land-use and land-cover (LULC). This territory is the primary source of water resources for a vast region in southern France and north-east Spain, feeding the runoff and recharge zones of the region's main catchment basins (Ebro, Adour, Garonne). Environmental changes can influence the availability of water resources, adding uncertainty to an already difficult water management situation due to high demand and variable supply, which can result in water scarcity situations that can last several years.

Several authors described the climate during the last decades in the Pyrenees including Morán-Tejeda et al. (2017) who found that

* Corresponding authors.
E-mail addresses: rclavera@obsebre.es (R. Clavera-Gispert), santiago.begueria@csic.es (S. Beguería).

https://doi.org/10.1016/j.ejrh.2023.101322
Received 28 July 2022; Received in revised form 13 January 2023; Accepted 22 January 2023
Available online 27 January 2023

increasing temperatures are responsible for a lesser accumulation of snow over time, López-Moreno et al. (2020) noted a snow cover decline, Pérez-Zanón et al. (2017) described the temperature trends in the central Pyrenees, Lemus-Canovas et al. (2019) described a statistically significant tendency towards a decrease in precipitation, and Vicente-Serrano and López-Moreno (2006) noted an increase in winter drought conditions in the eastern Pyrenees. Thus, in this climate change context, it is especially important to assess possible changes in the water cycle, particularly in surface flows, as stressed by several authors. García-Ruiz et al. (2001), and López-Moreno et al. (2011) detected a statistically significant decrease in the annual river contributions to the central south Pyrenees and the Ebro basin, respectively. Likewise, Zabaleta et al. (2019) detected a downward trend during all seasons in the basins close to the Bay of Biscay (western Pyrenees), although in the last 20 years the average discharge increased in winter and spring. In the French side of the Pyrenees, Le Treut (2013) reported a discharge decrease of 25–30% in the Garonne River, and Lespinas et al. (2010) and Labrousse et al. (2020) detected downward annual streamflow trends in the Northern coastal Mediterranean rivers. Stahl et al. (2010) also detected decreasing streamflow trends in two northern Pyrenean basins for the period 1952–2004.

In addition to climatic circumstances, non-climatic factors such as changes in land use can also strongly affect river flows. Beguería et al. (2003) estimated that 25% of streamflow decrease was caused by revegetation during the period 1945–1995 in the south-central Pyrenees. Likewise, Gallart and Llorens (2003) estimated that 30% of the streamflow decrease in the Ebro basin during the period 1945–1995 was due to an increase in evapotranspiration. Similarly, Buendia et al. (2016) ascribed the streamflow decrease to the combined action of climate change and afforestation in three sub-basins of the southern-eastern Pyrenees for the period 1987–2009. Finally, López-Moreno et al. (2006) and Vicente-Serrano et al. (2021) also studied the predominantly negative streamflow trends in the central-southern Pyrenees and ascribed them to a combination of climate change and afforestation.

The main method for describing the hydrological regime of watercourses is by means of gauging station streamflow records. When these records cover a sufficient period of time and are supplemented with tools such as hydrological modeling, they can also be used to evaluate, quantify, and interpret possible hydrological changes over time, as well as trends in water resource availability. Long time series (several decades) to study climate trends are needed to discern if the cause of the observed changes is due to natural variability or anthropic climate change. However, to separate the effects of LULC and those of climate, without discriminating between natural and human induced changes in climate, does not need time series as long, at least in the Pyrenees where the abandonment of agricultural areas has been rather fast (Lasanta et al., 2021).

Hydrological modeling helps to understand the underlying processes by simulating variables that are difficult or impossible to observe such as soil moisture, snowpack dynamics, or land evaporation. Modeling also allows performing numerical experiments impossible to conduct in the real world such as fixing land use to assess the impacts of climate change only (Quintana-Seguí et al., 2021). However, all those valuable contributions are subjected to model uncertainty, an issue that should not be neglected and thus be carefully assessed. Model uncertainty can be due to the model structure (how the physical processes have been represented in the model) and also due to the physiography, which often is fixed in models, while it changes in time in the real basin.

The objective of this study is to evaluate if models that correctly simulate the streamflow of the Pyrenees (in terms of KGE) are able to correctly simulate the observed streamflow trends. This article characterizes the recent evolution (1980–2013) of river streamflow in the Pyrenees, analyzing streamflow time series of several gauging stations and compare them with model simulations. Two hydrological models (SASER and SWAT) are used with different complexity and operating principles to analyze the uncertainty arising from the assumptions and errors of the models themselves and estimate the confidence in the results. The agreement and disagreement of the models with the observations and between them enriches the discussion of the observed streamflow evolution, and the attribution of the possible changes, which can have climatic or non-climatic origins (i.e., LULC), as well as the detection and quantification of the main sources of uncertainty. In this case the time period studied is short and, thus, unable to disentangle the effects of the natural variability of climate (due to decadal to centennial oscillations) but it is enough to disentangle the effects of climate (which affects both models and reality) and LULC (which is not simulated by these models).

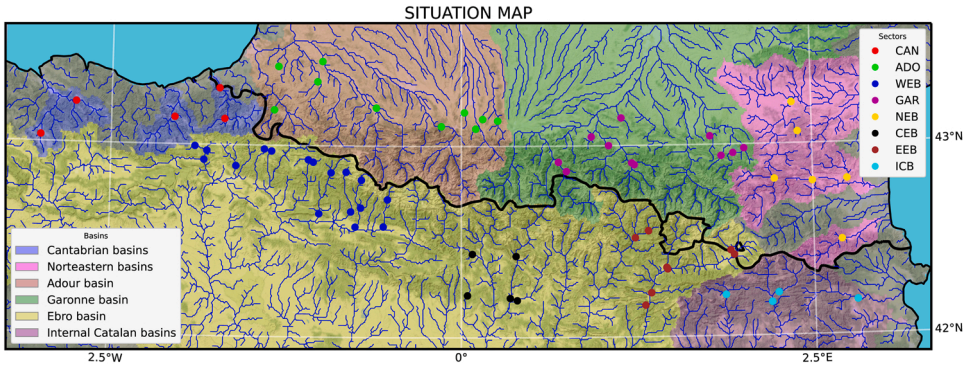

Fig. 1. Domain under study. Black lines are the coastline and the country borders. The watercourses are in blue. The filling colors are the basins and the colored dots are the gauging stations by region as in Table 1.

1.1. Study area

The Pyrenees has a rugged relief that stretches approximately 415 kilometers from west to east, from the Atlantic Ocean to the Mediterranean Sea, and 150 kilometers wide along its north-south axis. It encompasses the basins of the Ebro River, which flows into the Mediterranean Sea, the Adour and the Garonne Rivers, which flow into the Atlantic Ocean, as well as all other smaller basins surrounding them (Fig. 1). This singular geographical configuration confers the region a great climatic diversity, giving the Pyrenees a high environmental value.

The hydrographic network is characterized by numerous watercourses which generally adopt a north-south disposition, although some stretches are aligned in a west-east direction. In addition, the Pyrenees, as a natural "water tower", is the major source of water resources to the surrounding regions, providing the water needs of more than 15 million people and supplying electricity and irrigation water to a vast territory.

The climatic water balance (difference between annual precipitation and atmospheric moisture demand) in the Pyrenees is essentially positive, suggesting an absence of aridity and a clear water surplus, with values above 1000 mm per year in most of the area, especially near the watersheds and on the northern slope. On the other hand, the adjacent plains show much lower and even negative values, most notably to the south. Therefore, the rivers descending from the Pyrenees are the main source of water resources in these surrounding areas.

Annual precipitation presents important contrasts, ranging between 500 and 3000 mm per year. Precipitation is spatially distributed according to a west-east gradient, which is related to the generation of precipitation by the humid Atlantic air masses. Also, there is the altitudinal gradient, with increasing precipitation as altitude increases. Thus, the maximum annual precipitation values are concentrated on the Atlantic coast, while the lowest values are found towards the Mediterranean and in the interior depressions and foothills. On the northern slope, moreover, the Atlantic influence extends from the piedmont zone to the central sector, increasing the Mediterranean influence towards the piedmont zones and towards the east.

The seasonal rainfall regime has a very pronounced minimum in the summer months and a secondary minimum in winter. The maximums occur in autumn and spring. There are, however, important differences between sectors, with a gradient again appearing from west to east. Thus, in the westernmost valleys, the most important maximum is in autumn, while the spring maximum is secondary. On the other hand, in the eastern valleys the main maximum is the spring one, while the autumn maximum is less pronounced. There are also differences in the minimums since towards the west the main minimum occurs in summer while in the easternmost valleys the winter minimum is more pronounced. The transition between the two regimes occurs gradually as the Atlantic influence leads way to the Mediterranean one.

In this work, the Pyrenees is divided into 8 sectors (Fig. 1 and Table 1), according to geographical and water management criteria. The Ebro basin is the largest of the Pyrenees and collects water from the western to the eastern part of the mountain range, so it is subdivided into 3 parts: western (WEB), central (CEB) and eastern (EEB) Ebro tributaries. On the other hand, the little basins in the Cantabrian area are grouped in a single region (CAN), as well as the basins in the southeastern Pyrenees (internal Catalan basins: ICB) and the northeastern basin (NEB). The Adour and the Garonne basins are each one a region (ADO and GAR, respectively).

2. Data and methods

2.1. Datasets

To achieve the objectives, observational data is needed to validate the models and assess the actual trends,. Beyond this data, meteorological forcing data (state of the atmosphere at each instant) and physiographic information (topography, soil texture, vegetation cover, land use, etc.) are also needed to feed the models. All datasets used are presented and described below.

2.1.1. Hydrological data observations

The region under study comprises three countries (Andorra, France, and Spain), and different administrative and management entities are involved in the administration of water resources. Streamflow data from these entities is collected, harmonized, and merged into a unique daily streamflow dataset named PIRAGUA_indicators (Zabaleta et al., 2022).

Not all the available data from gauging stations present in the study area were eligible to study streamflow evolution and trends. The main criteria to make the final selection of gauging stations are:

Table 1
Pyrenean regions used in this study and the number of gauging stations.

Basin	Abbreviation	Nº of gauging stations
Adour	ADO	10
Garonne	GAR	11
Northeastern	NEB	6
Cantabric	CAN	5
Ebro	WEB	17
	CEB	5
	EEB	9
Internal Catalan	ICB	4

1. Be in a natural or semi-natural regime (e.g., not influenced by dams or significant water extraction).
2. Do not present an altered hydrological regime (e.g., maximum flows in august).
3. Do not have abrupt changes in their time series.
4. Have more than 20 years of data, and do not have important gaps (such as complete year gaps).

From this preliminary work, a set of 67 quality time series from near-natural gauging stations geographically dispersed across the study area (Fig. 1).

2.1.2. Meteorological data

The hydrological models were driven with a common forcing dataset, the PIRAGUA_atmos_analysis dataset (Quintana-Seguí, 2022). It is a meteorological dataset based on SAFRAN (Système d′Analyse Fournissant des Renseignements Atmosphériques à la Neige; (Durand et al., 1993, 1999) that produces gridded datasets of screen-level meteorological variables by combining the outputs of a meteorological model and all available observations using an optimal interpolation algorithm. SAFRAN has been extensively used in France (e.g., Le Moigne et al., 2020; Quintana-Seguí et al., 2008; Vidal et al., 2010) and, more recently, it has also been applied in Spain (Quintana-Seguí et al., 2016, 2017), Tunicia (Tramblay et al., 2019), and Moroco (Moucha et al., 2020).

PIRAGUA_atmos_analysis was performed by taking the results of the optimal interpolation step of the French and Spanish SAFRAN datasets and doing the final step of interpolation anew, using a common grid that covers the study area (enlarged Pyrenees, including all the basins that drain the range) (Fig. 2). The result is a gridded dataset of temperature, precipitation, relative humidity and wind speed that covers the area limited by 370000 m and 1085000 m in the y-axis, and 4465000 m and 5080000 m in the meridional axis according to the UTM projection ETRS89 datum 30 N (EPSG: 25830), with a spatial resolution of 2.5 km and hourly time resolution.

2.1.3. Radiation data

ERA5 (ECMWF) (Hersbach et al., 2018) was used for radiation when creating PIRAGUA_atmos_analysis from SAFRAN Spain and SAFRAN France, because radiation values were not consistent with each other. ERA5 covers the Earth on a 0.25° resolution grid. These data have been interpolated to the same grid as the PIRAGUA_atmos_analysis dataset.

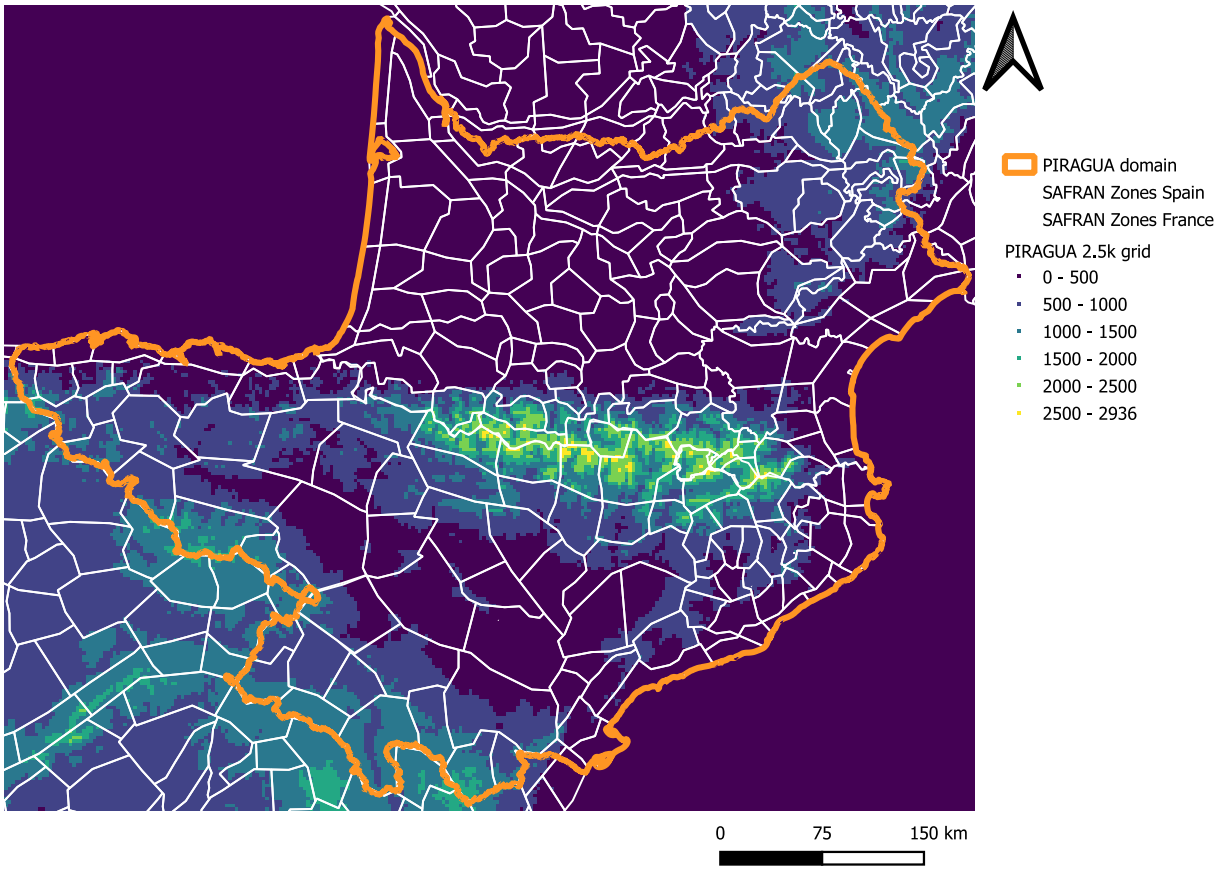

Fig. 2. PIRAGUA_atmos_analysis domain that covers the PIRAGUA region and the surrounding basins (orange region). The white lines delimit meteorologically homogeneous zones used by the SAFRAN algorithm. The graded colors are the altitude in a 2.5 km grid.

2.1.4. Other data

Additional input data was required for simulations of the region such as topography and land cover, which were obtained from several sources (Table 2). It should be noted, as it will be relevant for the discussion of the results, that these parameters are considered constant in time during the simulations.

2.2. Hydrological modeling

As mentioned above, this work used the results of the two hydrological models (SASER and SWAT) over the Pyrenees for the period 1981–2010, which are grouped in a dataset named PIRAGUA_hydro_analysis (Beguería et al., 2022).

These two models present different complexity and operational principles, allowing to evaluate the results' uncertainty and confidence level and both have been applied to several case studies and have a proven track record, including Choudhary and Athira (2021), Cui et al. (2021), Datok et al. (2021), and Olaoye et al. (2021) for SWAT; and Guinaldo et al. (2021), Tóth and Szintai (2021), and Vural et al. (2021) for SURFEX. A brief introduction to these models is given here, but for more details about the theory and implementation the reader is directed to their web pages: http://www.umr-cnrm.fr/surfex/ (last access: 13/12/2022), and https://swat.tamu.edu/ (last access: 13/12/2022).

2.2.1. SASER

The full modeling platform SASER (SAfran-Surfex-Eaudysee-Rapid) is formed by a meteorological dataset based on SAFRAN (already presented above), the land surface model SURFEX, RAPID, and EAU-DYSEE, which will be introduced below. The SASER term will be used throughout this work, following previous examples (Bhuiyan et al., 2018; Gaona et al., 2022; Quintana-Seguí et al., 2020).

2.2.2. SURFEX

SURFEX (SURFace EXternalisée) is Météo France's surface modeling platform (Le Moigne et al., 2020; Masson et al., 2013). It is a physical and fully distributed land surface model using a regular grid and computes the hydric and energy balance in continental surfaces. For natural soils, SURFEX uses the ISBA (Interaction Sol-Biosphère-Atmosphère) land surface scheme (Noilhan and Mahfouf, 1996; Noilhan and Planton, 1989). The ISBA scheme calculates the surface energy and water budgets over natural areas. There are different versions of ISBA, but ISBA-DIF is used in this study, which is the multi-layer diffusion version (Boone et al., 2000; Habets et al., 2003). SURFEX lacks a native routing scheme, but it can use RAPID (Routing Application for Parallel ComputatIon of Discharge; (David, Cédric H, 2013) as a routing model, and the connection between SURFEX and RAPID being Eau-dysée (both tools are described below).

2.2.3. RAPID

Since SURFEX has no river routing scheme, RAPID (David et al., 2011) is chosen to do this. RAPID transfers SURFEX's total runoff (surface and subsurface or drainage) from the SURFEX grid cells to the river cells using its own isochrony algorithm. Then, RAPID uses a matrix-based version of the Muskingum method to calculate flow and volume of water for each reach of a river network. As the current setup cannot simulate dams, canals, or irrigation, the resulting river flows are estimations of the natural system (that is, the system without direct human intervention in the form of irrigation or hydraulic infrastructures, such as dams or canals).

2.2.4. EAU-DYSSÉE

Eau-dyssée is a framework that couples hydrological models (Flipo et al., 2012; Saleh et al., 2011), in this case SURFEX and RAPID, managing the different space and time scales, and exchanging the appropriate variables between them.

2.2.5. SWAT

SWAT (Soil and Water Assessment Tool; (Douglas-Mankin et al., 2010) is a semi-distributed basin-scale time-continuous hydrological model supported by the USDA Agricultural Research Service. The minimum requirements for SWAT include topographic, land use / land cover, soil, and climate data. As SWAT simulates at the basin-scale, the study area was divided into 20 basins (Fig. 3), and in turn, as a semi-distributed model, the catchment was divided into sub-basins, which are further divided into hydrological response units (HRUs), which are homogeneous units of land use, soil type, and slope. The basin discretization into sub-basins is based on the

Table 2
Additional data used in the SASER and SWAT hydrological models.

	SASER	SWAT
Topography	GTOPO-30 (Earth Resources Observation And Science (EROS) Center, 2017)	Shuttle Radar Topography Mission (Jarvis et al., 2008) European DEM v.1.1 (land.copernicus.eu/imagery-in-situ/eu-dem/eu-dem-v1.1; last acces: 4/07/2022)
Land use	ECOCLIMAP (Faroux et al., 2013; Kaptue Tchuente et al., 2010)	Corine (Büttner, 2014) Mapa cobertes del sòl d'Andorra (iea.ad/mapa-de-cobertes-del-sol-d-andorra-2012; last acces: 4/07/2022)
Soil		Harmonized world soil database (Wieder et al., 2014)
Hydrographic net	HydroSHEDS (Lehner et al., 2008)	

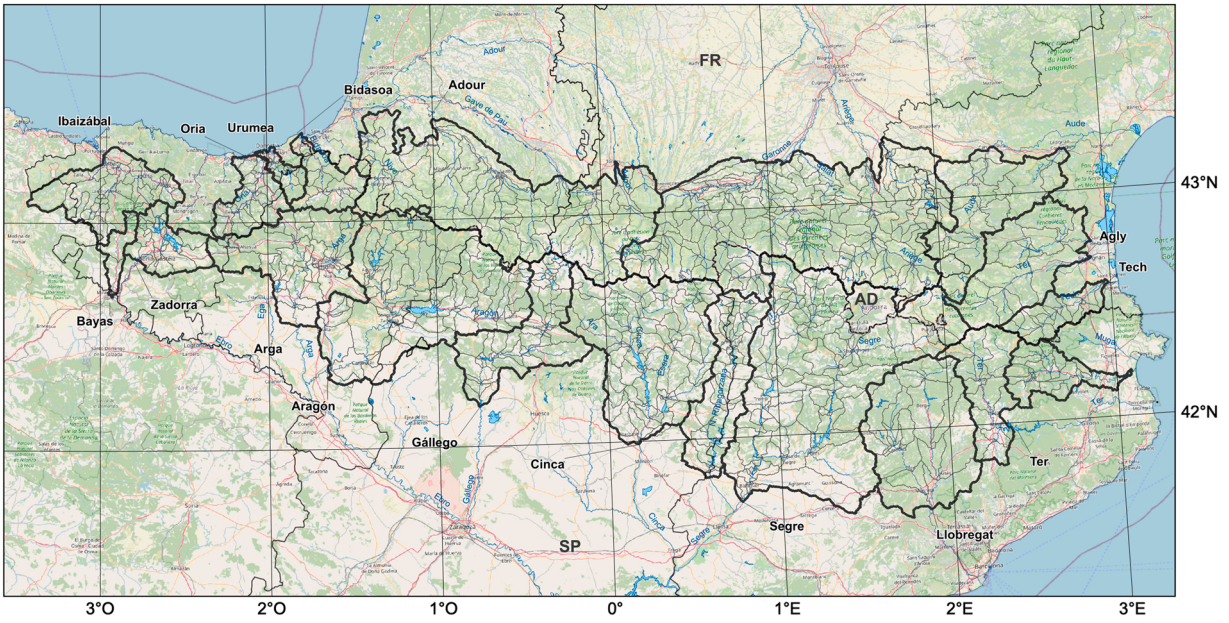

Fig. 3. Division of the Pyrenees in basins and subbasins as they have been simulated by the SWAT model. These are SWAT projects that are further divided into smaller subbasins (basemap from OpenStreetMap).

catchment areas as defined in the European system (Directive 2000/60/EC). These sub-basin limits coincide with the gauging stations where the calibration, validation, and model analysis should be carried out.

The SWAT system, as a conceptual model, requires calibration and validation. The corresponding time periods were model initialization (warm-up), 1980–1985; calibration, 1986–2005; and validation, 2006–2013.

The sensitive parameters were identified and calibrated using the literature of the region (Biancamaria et al., 2019; Cakir et al., 2020; Grusson et al., 2015, 2017a, 2017b, 2018; Martin et al., 2016). The main calibration target was objective function KGE optimization. For this, the Sequential Uncertainty Fitting (SUFI-2) algorithm (Abbaspour et al., 2004) was used because this method identifies an optimal parameter set in a limited number of iterations (Yang et al., 2008).

The calibration was made in 2 stages: first, a calibration with all stations together, to find a general equilibrium of the sensitive parameters over all basins. The second stage consisted of a separate calibration of those stations where the simulation performance was insufficient to adapt the calibration to the local particularities.

Once the SWAT model was calibrated and validated, the resulting parameters and configuration was applied to the full period (1980–2013), to compare the models' results with observed streamflow series from the gauging stations. Due to the system requiring an initialization period, the first five years of data (1980–1985) were artificially replicated to apply them to the period 1975–1979 and ensure a modeling period from 1980 to 2013.

2.3. Methodology

2.3.1. Goodness-of-fit

The performance of the simulated daily streamflow time series was evaluated using the non-parametric variant of the Kling-Gupta efficiency test (KGE_{NP}; (Pool et al., 2018). This statistic considers different types of model errors, namely the error in the mean, the variability, and the dynamics (Pool et al., 2018). The calculation of KGE (standard parametric version) is implicitly based on the assumptions of data linearity, data normality, and the absence of outliers, but the streamflow time series do not necessarily follow these assumptions, for this reason the non-parametric version of KGE is used in this study.

$$KGE_{NP} = 1 - \sqrt{(r_s - 1)^2 + (\alpha_{NP} - 1)^2 + (\beta - 1)^2} \tag{1}$$

$$\alpha_{NP} = 1 - \frac{1}{2}\sum_{k=1}^{n}\left|\frac{Q_{sim}(I(k))}{n\overline{Q}_{sim}} - \frac{Q_{obs}(J(k))}{n\overline{Q}_{obs}}\right| \tag{2}$$

$$\beta = \frac{\mu_{sim}}{\mu_{obs}} \tag{3}$$

$$r_s = \frac{\sum_{i=1}^{n}(R_{obs}(i) - \overline{R}_{obs})(R_{sim}(i) - \overline{R}_{sim})}{\sqrt{\left(\sum_{i=1}^{n}(R_{obs}(i) - \overline{R}_{obs})^2\right)\left(\sum_{i=1}^{n}(R_{sim}(i) - \overline{R}_{sim})^2\right)}} \quad (4)$$

The function is computed from three parameters: the Spearman's rank correlation as an indicator of general goodness of fit (r_s), where R_{obs} and R_{sim} are the ranks of the observed and simulated discharge time series respectively; the normalized flow–duration curve (FDC) as an indicator of discharge variability (α), where *I(k)* and *J(k)* are the time steps when the *k*th largest flow occurs within the simulated and observed time series, respectively; and the quotient of the means division as an indicator of bias (β). The KGE_{NP} ranges from -infinity < $KGE_{NP} \leq 1.0$, being $KGE_{NP} = 1.0$ the perfect agreement between simulations and observations. There is no benchmark from which a simulation is considered 'good' or 'bad' (Knoben et al., 2019), although Knoben et al. (2019) consider that the model has predictive capacity if KGE_{NP} between the observations and the simulation is greater than the KGE_{NP} between the observations and their mean. The python package Hydroeval (Hallouin, 2021) was used to compute the KGE_{NP}.

On the other hand, the simulations made with SWAT need to be calibrated and validated, therefore the KGE_{NP} can only be applied to the validation period. Consequently, the KGE_{NP} for the SWAT simulations were calculated for the period 2006–2013. This is not the case for SASER because it does not need calibration. Therefore, the validation between observations and simulation could be performed over the whole modeled period (1980–2013). To make KGE_{NP} comparable, the 2006–2013 period for both models is used.

2.3.2. Trend calculation

Daily time series of observations and simulations were transformed to monthly and seasonal descriptive statistics (quantiles: Q10, Q50, Q90) and annual time series. The statistics Q10, Q50 and Q90 are chosen, which are the thresholds that are not surpassed during 10%, 50% or 90% of the time respectively, as proxies for low (Q10), medium (Q50) and high (Q90) flows. These statistics were calculated for both of the study periods: 1980–2013 period, and 1990–2013 period and for all gauging stations to evaluate their trends over time.

The existence of a trend in a time series can be detected by several statistical tests (Bayazit, 2015). The Sen's slope estimator (Sen, 1968) is used is this study, assuming a linear trend over time. The significance of the trends was assessed with the rank-based non-parametric Mann-Kendall test (MK; (Mann, 1945), which is the most widely used for trend analysis in hydrology. Before the test, a pre-whitening of the series is applied using the Collaud Coen et al. (2020) methodology and Vogt (2021) software library, which involves three pre-whitening methods. The purpose of pre-whitening is to eliminate from the analysis the influence of likely temporal autocorrelation in the data, which would cause inflation of the statistical significance values and, therefore, generate a higher than expected number of false positives. MK is applied on the pre-whitened series at the 95% significance level ($p < 0.05$).

2.3.3. Graphical representation of trends

As an aid to the interpretation of the trends, a graphical representation of the trends is designed (Fig. 4). The plot represents points

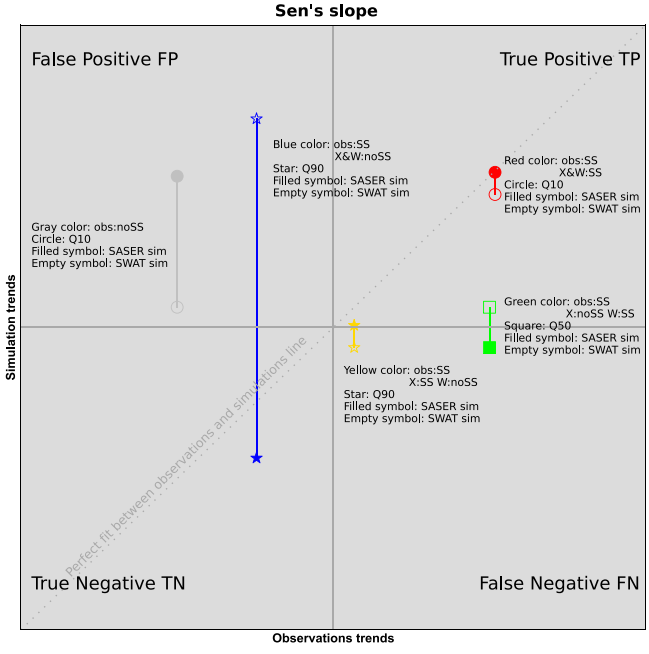

Fig. 4. Graphical representation of observed and simulated trends. Detailed description in text.

on a two-dimensional plane, where the x-axis and y-axis correspond to the value of observed and simulated trends, respectively. Therefore, there will be two points for each observed trend, one for SASER (filled symbol in Fig. 4) and one for SWAT (empty symbol in Fig. 4). These two symbols are joined by a vertical line representing a proxy of the simulations' uncertainty. The shape of the symbol represents the statistic (Q10 is a circle, Q50 is a square, and Q90 is a star). The color of the symbol represents the statistical significance (Fig. 4), being gray when there is none, red when both observations and simulations are significant, blue when observations are statistically significant, but simulations have no statistical significance, and green when the observations and SWAT have statistical significance and yellow when the observations and SASER have statistical significance.

Points in the quadrant delimited by the upper right continuous gray lines represent positive trends in both observations and simulations (equivalent to TP of M), while points in the lower left quadrant represent negative trends in both observations and simulations (equivalent to TN of M). In these two cases, the closer to the dashed line the more similar is the slope of the simulations and the observations. On the other hand, the FP of M are in the upper left quadrant, and the FN are in the lower right quadrant.

3. Results

3.1. Simulation performance

The validation results are summarized in Fig. 5. Regarding the validation of SASER at the daily time step, and considering the criteria previously established in the methodology, more than 89% of the simulations had a better skill than the one obtained using the mean of the time series, with a median value of $KGE_{NP} = 0.44$. This percentage increased with SWAT, reaching over 98% with a median of $KGE_{NP} = 0.51$.

At the seasonal level, the median performance ranged between 0.39 (summer) to 0.55 (winter) for SASER, and between 0.46 (autumn) to 0.64 (spring) for SWAT. The SASER KGE_{NP} is better than using the mean in more than 77% (winter) cases, being the maximum 92% (summer). For SWAT, the KGE_{NP} ranged between 0.46 (autumn) to 0.64 (spring), with the best results in winter and spring (98%) and the worst in autumn (91%).

Considering months, the percentages ranged between 70% (Sep.) to 92% (Jul.) for SASER, and between 58% (Sep.) to 97% (Dec., Jan. and Jun.) for SWAT, with median KGE_{NP} ranging between 0.17 (Aug.) to 0.58 (Nov.) for SASER and between 0.08 (Aug.) to 0.64 (Jan.) for SWAT.

Going back to the annual scores, one sees that:

- The r_s (discharge dynamics indicator) ranged between 0.05 and 0.97 for SASER and between − 0.52 and 0.95 for SWAT. In most cases there is a moderate to strong positive association in both models (although in SWAT there are 5 out of 1139 cases with negative values).

- The α values (discharge variability) of observations and simulations ranged between 0.98 and 0.38. This indicates short discharge variability between simulations and observations.
- In contrast, unlike the two previous parameters, β values showed clear differences between models. SASER values ranged between 58.0 and 0.1, while for SWAT ranged between 9.7 and 0.1 (Fig. 5). Therefore, the β parameter was the one that most clearly conditioned the final KGE_{NP} value and is the one that made SWAT models give better overall skill. Although, it should be noted that during simulations SASER conserves all the simulated water, but SWAT can calibrate a variable that determines the amount of water that quits the system through deep percolation and thus determines the discharged volume (β).

In general, the best fits between observations and simulations were obtained in winter and spring, while the worst fits were during summer and autumn (Table 3). This is expected, as hydrogeology plays a more relevant role in sustaining streamflow during summer,

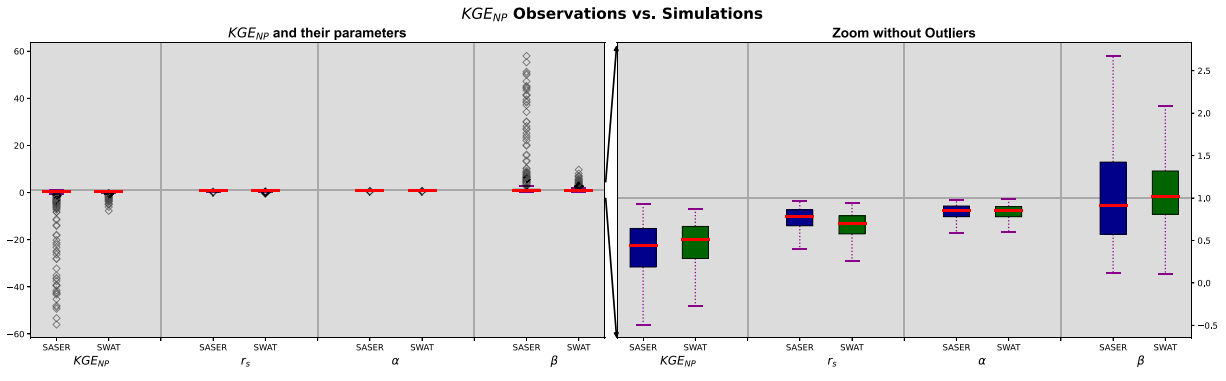

Fig. 5. KGE_{NP} of SASER and SWAT, and their components. Left box plot shows the results with outliers, while the right box plot zooms the results without the outliers. The blue color is SASER and the green color is SWAT.

Table 3
Median of KGE_{NP} computed for each region for both models (SASER: SR and SWAT: SW) each month and season.

	TOTAL		ADO		CAN		GAR		WEB		CEB		EEB		NEB		ICB	
	SR	SW	SR	SW	SR	SW	SR	SW	SR	SW	SR	SW	SR	SW	SR	SW	SR	SW
Sep.	0.21	0.09	0.05	0.34	0.08	-0.41	0.04	0.32	0.45	0.01	0.38	0.09	0.24	-0.07	-0.34	-0.31	0.19	0.33
Oct.	0.37	0.33	0.49	0.44	0.37	-0.18	0.24	0.37	0.60	-0.04	0.56	0.32	0.36	-0.04	0.28	0.17	0.36	0.36
Nov.	0.58	0.53	0.77	0.59	0.53	0.53	0.49	0.58	0.55	0.63	0.70	0.50	0.31	0.48	0.50	0.19	0.48	0.47
Dec.	0.54	0.58	0.64	0.61	0.64	0.73	0.50	0.68	0.41	0.58	0.73	0.57	0.11	0.34	0.51	0.45	0.44	0.26
Jan.	0.53	0.64	0.71	0.70	0.71	0.76	0.59	0.76	0.29	0.62	0.60	0.51	0.06	0.18	0.52	0.70	0.61	0.42
Feb.	0.48	0.61	0.67	0.70	0.77	0.77	0.67	0.81	0.18	0.56	0.50	0.49	0.05	-0.01	0.73	0.72	0.68	0.55
Mar	0.57	0.63	0.72	0.66	0.82	0.71	0.53	0.62	0.53	0.61	0.35	0.27	-0.55	0.33	0.40	0.67	0.67	0.68
Apr.	0.43	0.52	0.70	0.60	0.64	0.68	0.39	0.55	0.44	0.56	0.58	0.21	0.14	0.33	0.09	0.40	0.43	0.33
May	0.47	0.56	0.58	0.66	0.74	0.66	0.35	0.54	0.57	0.60	0.44	0.53	0.42	0.39	0.29	0.00	0.44	0.50
Jun.	0.45	0.58	0.58	0.58	0.69	0.60	0.34	0.62	0.59	0.60	0.38	0.65	0.62	0.58	0.27	0.48	0.42	0.51
Jul.	0.30	0.37	0.23	0.52	0.24	0.37	0.20	0.38	0.43	0.09	0.18	0.12	0.38	0.47	0.11	0.29	0.33	0.51
Aug.	0.17	0.08	0.11	0.35	0.16	0.06	0.09	0.21	0.28	-0.06	0.09	0.01	0.20	0.03	-0.05	0.01	0.15	0.25
Autumn	0.47	0.46	0.61	0.54	0.50	0.30	0.39	0.51	0.60	0.49	0.66	0.35	0.35	0.22	0.42	0.17	0.39	0.42
Winter	0.55	0.63	0.70	0.66	0.70	0.76	0.66	0.75	0.38	0.62	0.64	0.53	0.27	0.21	0.63	0.68	0.63	0.45
Spring	0.53	0.64	0.66	0.71	0.65	0.64	0.37	0.65	0.62	0.63	0.60	0.64	0.46	0.58	0.41	0.62	0.45	0.54
Summer	0.39	0.50	0.39	0.59	0.52	0.38	0.27	0.51	0.56	0.50	0.30	0.60	0.59	0.59	0.18	0.39	0.34	0.44
Daily	0.56	0.65	0.73	0.71	0.75	0.69	0.46	0.66	0.62	0.64	0.60	0.66	0.35	0.53	0.50	0.65	0.47	0.54

and this was not simulated by the models.

Table 3 summarizes the results by region. The best scores were found in the western Pyrenees, ADO and CAN areas for the 2 models, while the worst were located in the EEB and NEB (Table 3). These regions have a marked Mediterranean character, and it is known that these models perform worse in a Mediterranean context (Merheb et al., 2016). Looking seasonally, the highest values are found in all basins in winter and spring, and the lowest are in summer for SASER and autumn for SWAT. The only exception is the EEB, which had lowest values in winter and maximum values in summer. The worst values were in September and August. The highest values were more dispersed, and in general were found in the winter months (DJF).

Therefore, a spatial and temporal distribution of the KGE_{NP} can be seen with higher values in wetter areas and lower values in drier areas, with dry months showing the worst values and wetter months showing the best values. Thus, the models work better in the wetter climates and for the rainier seasons, because they simulate rainfall-runoff processes better (except the extreme ones) than the always more complex hydrogeology that is predominant in summer.

3.2. Comparing time periods

Focusing on the 1980–2013 time period (Fig. 6; for a detailed representation see Supplementary material), out of the 804 measurements (for all the gauging stations, for 4 seasons and the 3 statistics: Q10, Q50 and Q90) 89.8% of the observed time series do not have significant trends. Considering only the 82 observed significant trends, 76.8% of these did not achieve statistical significance in the simulations by either model. 20.7% were captured by SWAT but not by SASER (mainly in the Q50), and only 1.2% were simulated by SASER and not by SWAT. Observed trends with statistical significance simulated by both models represent 1.2%. Also, the season with the least statistically significant trends is winter (11%) and the one with the most is autumn (33%), while spring and summer have similar values (27% and 29% respectively). The quantile with the highest number of significant trends was Q50 (39%), followed by Q10 (38%) and finally Q90 (23%). Therefore, the conclusion is that the simulations had poor skill in predicting the significant observed streamflow trends during 1980–2013 period.

Similarly, during the 1990–2013 time period 89.2% of the observed time series showed no significant trends (Fig. 7; for a detailed representation see Supplementary material). Taking into account only the significant trends, 58.6% of these were not simulated with statistical significance by either model, 13.8% were captured by SWAT but not by SASER, and 9.2% were simulated by SASER and not by SWAT. Observed trends with statistical significance simulated by both models represented 18.4%. Also, the season with the least observed significant trends is spring (14.9%) and the one with the most is autumn (46%), while winter and summer have similar values (20.7% and 18.4% respectively). The statistical parameter with the highest number of significant trends is Q10 (43.7%), followed by Q50 (41.4%) and finally Q90 (14.9%). The simulations, again, showed poor skill in predicting the observed streamflow trends during this period.

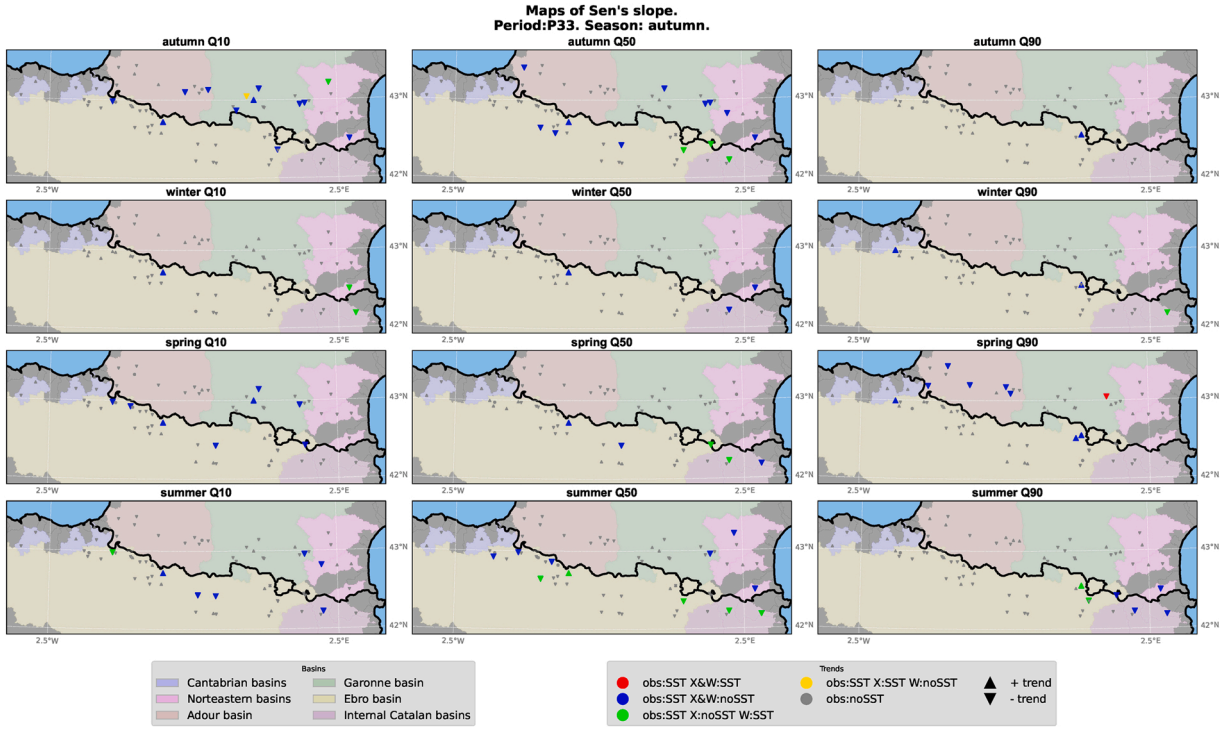

Fig. 6. Trend maps by season (rows) and percentile (columns) for the 1980–2013 (P33) period. Monthly distributions are in the Supplementary material.

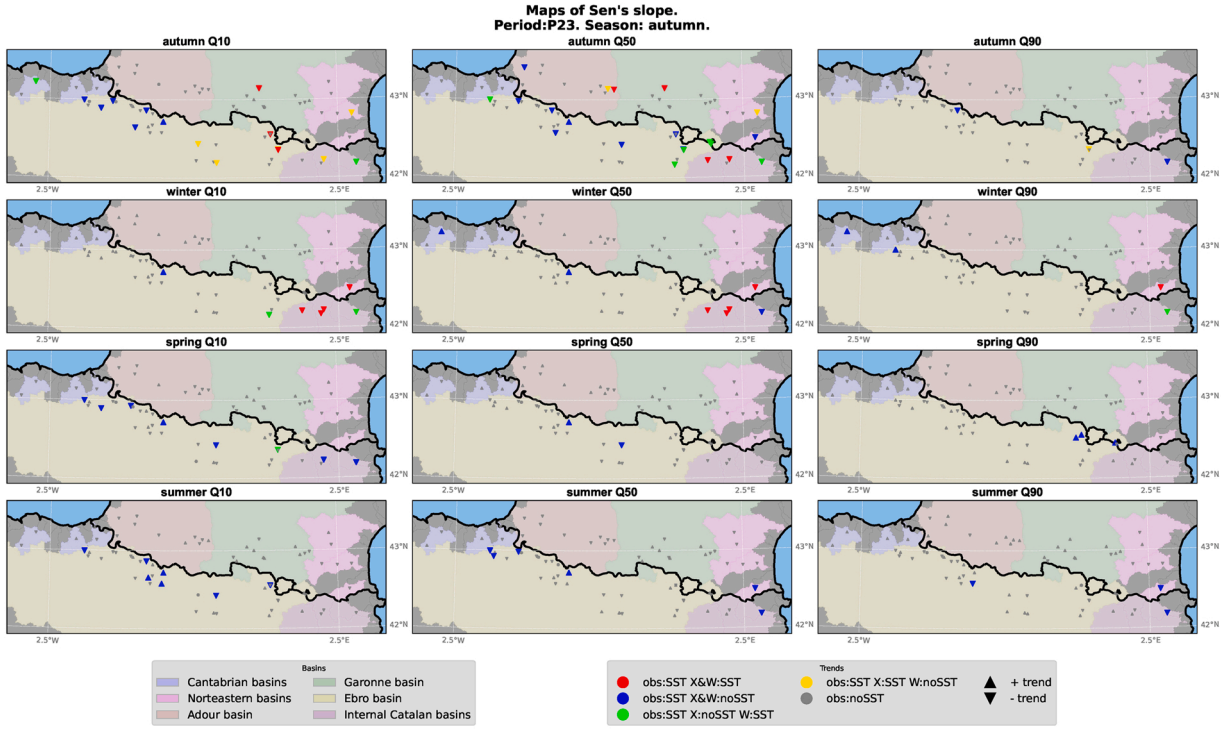

Fig. 7. Trend maps by season (rows) and percentile (columns) for the 1990–2013 (P23) period. Monthly distributions are in the supplementary material.

3.3. Seasonal distribution of the trends

During autumn (Figs. 6 and 7; for a detailed temporal and regional distribution of the trends see Supplementary material), the observations show a clear negative significant trend signal throughout the Pyrenees. This is especially true for the eastern part (EEB and ICB), where the simulations show these trends in the 1990–2013 period. As for the western parts, simulated significant trends appear in this period during September in WEB for Q90 (Fig. 8) and October in GAR for Q10 (Fig. 9).

Throughout winter (Figs. 6 and 7), the observations and simulations in the south-eastern areas (EEB and ICB) have negative significant trends in the 1990–2013 period. This is in contrast to the trends observed during this season in the western sectors (CAN and WEB) where they can be positive in this period, especially in February's Q90.

Spring is the season with more variability, presenting positive and negative significant trends. There is no clear pattern in the 1980–2013 period, but in general terms, it is observed that observations from the northern half have negative significant trends (which are not simulated) while in the southern sector (WEB, CEB and EEB) they have positive significant trends. The ICB sector does not mainly present significant trends, but when the observations have significant trends, these are negative. For the 1990–2013 period, northern sectors do not mostly present significant trends, except for CAN that shows them, as well as the southern slope positive significant trends in the observations, which are also simulated in the CAN and WEB (Fig. 10).

The significant trends distribution in Summer shows negative values in observations affecting the Mediterranean basins (mainly CNE and ICB, but also the Eastern gauging stations of EEB and GAR). For the 1990–2013 period, the Northern half, with the exception of those already mentioned, has hardly any significant trend, and the observed in the southern slope, despite having some positive values, are mostly negative.

Overall, the sectors most affected by negative significant trends are located in the Mediterranean area, especially the southern slope, with negative values in all seasons, with peaks in autumn and winter. On the contrary, the sectors less affected by negative significant trends are those located in the northern slope (except for NEB), that even have positive significant trends in March in CAN. This allows to see a distribution of trends by slope on the East-West axis, finding the extremes in ICB and CAN.

3.4. Distribution of the trends by statistics

Q10, that is the low flows, is the statistic that presents more significant trends, followed by Q50, and finally Q90, mostly in the autumn months. This distribution holds whether or not the trend has been correctly reproduced by the models, i.e., when the significant trend has been observed and simulated. The statistic with more significant trends is still Q10, followed by Q50 and Q90 also in autumn.

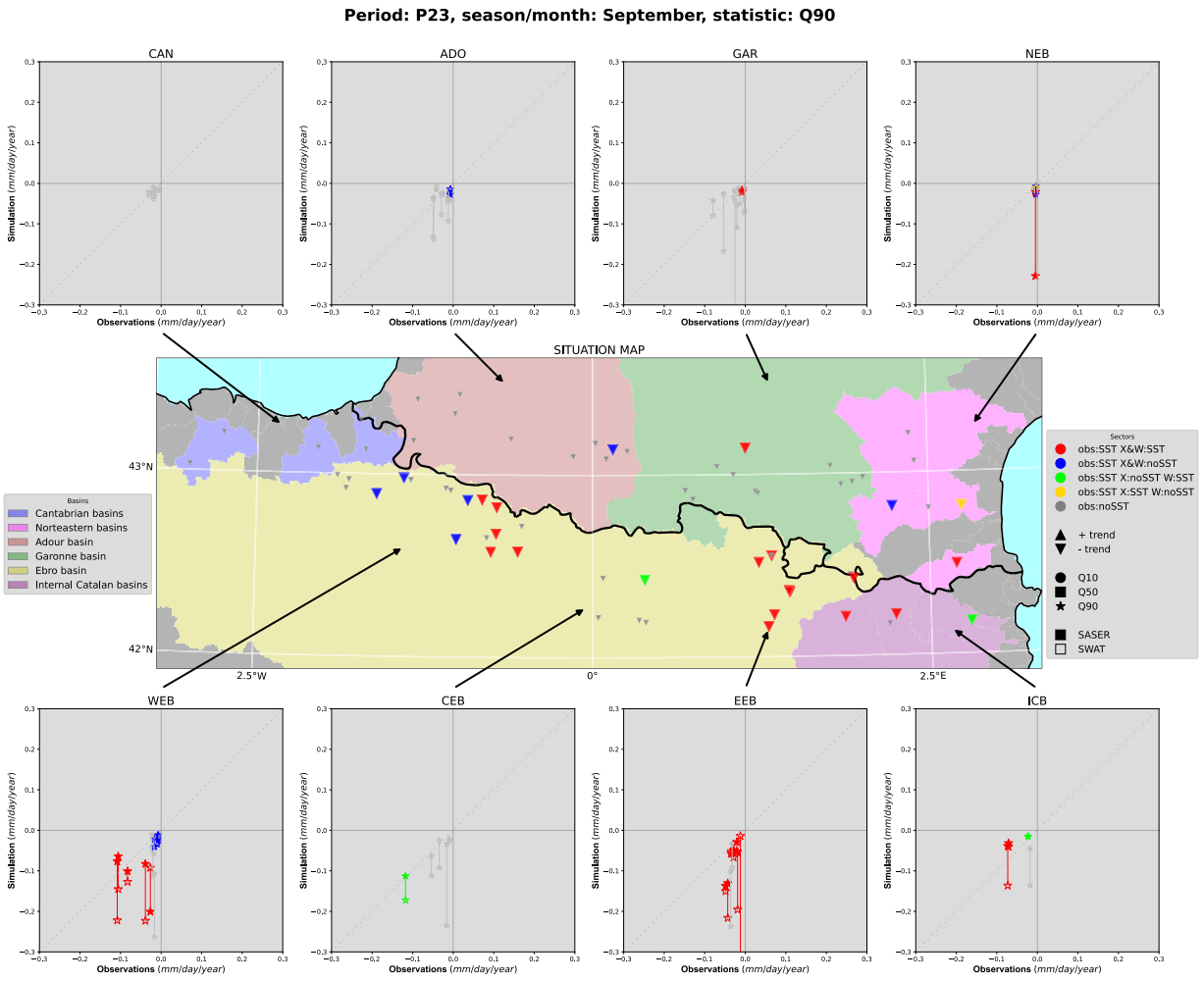

Fig. 8. Statistically significant trend distribution by regions in a map and their graphical representation for September, the Q90 percentile, and the 1990–2013 (P23) period. The negative significant trends (observed and simulated) are mainly located in WEB, EEB, and ICB. The negative only observed significant trends (not simulated) are mainly distributed in WEB.

Regarding the monthly distributions of quantiles (Fig. 11), a major number of negative significant trends in Q10 (low flows) are in October, this distribution is observable in both periods (1980–2013 and 1990–2013), as well as in observations and both simulations. On the other hand, positive trends are remarkable at February, March and especially April for the Q90 (high flows) in the 1990–2013 period, this distribution is not so marked in the simulations as in the observations.

3.5. Attributions of the trends

Streamflow trends can arise from a number of causal factors, but the attribution is not trivial. There are different combinations of situations depending on whether the trends can be observed and/or simulated:

- The most common scenario in this study is when there are not statistically significant trends in either observations or simulations (Fig. 12B). In principle, this should be interpreted as that there is no real increase or decrease in the river flow trend. However, it could be that there is a very subtle trend that is masked by noise, or that the method used to calculate the trend is not adequate to capture it.
- The easiest scenario to interpret is when significant trends are detected in both observations and simulations. In this case, this trend is attributed to the climate (i.e., EEB in September for the 1990–2013 period shown in Fig. 12A), because the models, which have fixed parameters and physiography, can only produce trends due to climate factors. However, there will always be a difference between the observed and simulated values due to model limitations or to other non-climatic factors affecting the observed trends that are not simulated by the models (e.g., WEB in September for the 1990–2013 period, January of NEB in the 1990–2013 period).

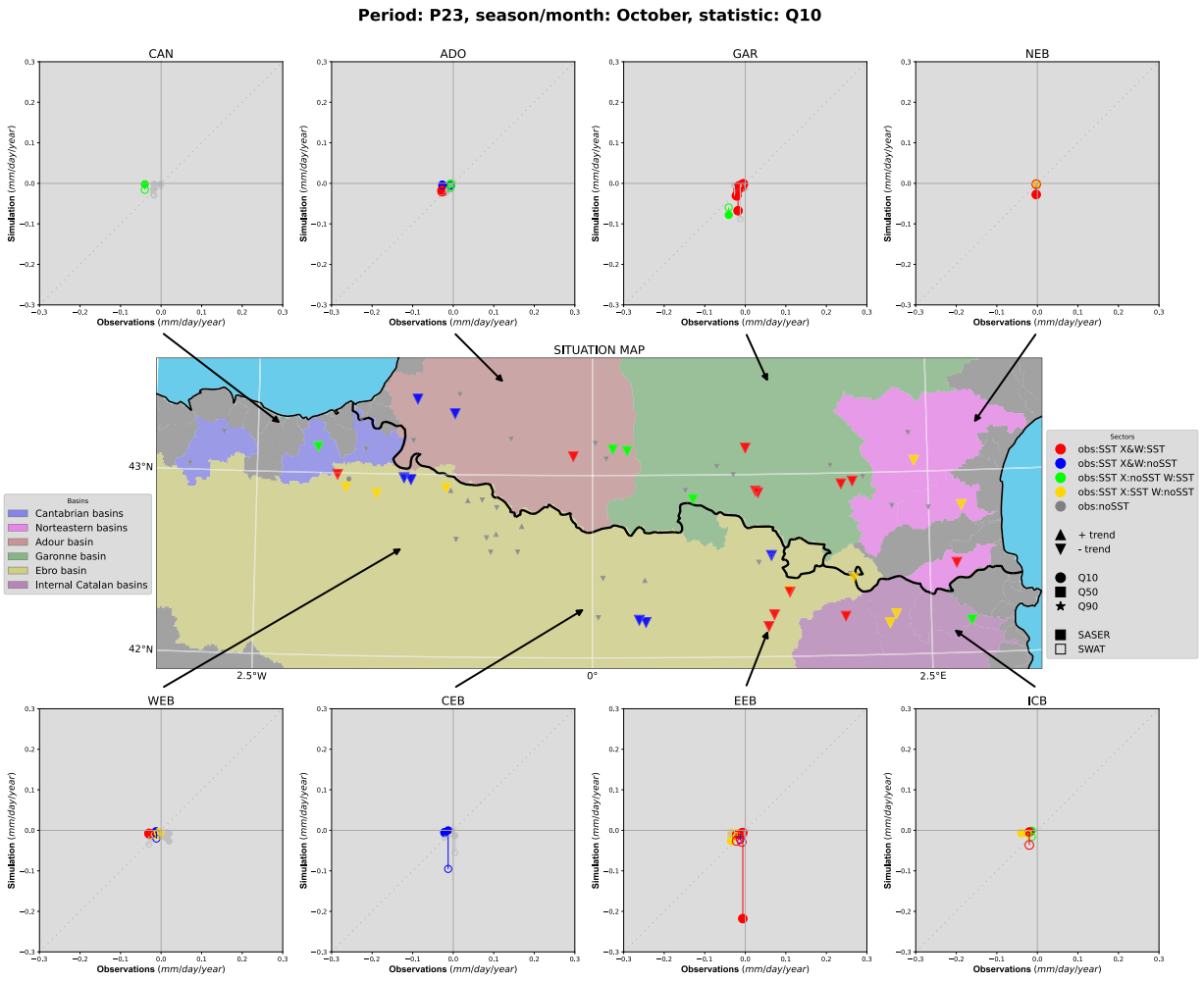

Fig. 9. Statistically significant trend distribution by regions in a map and their graphical representation for October, the Q10 percentile, and the 1990–2013 (P23) period. The negative significant trends (observed and simulated) and just observed significant trends (not simulated) are distributed in all regions.

The distance between simulated trend values (red lines joining symbols in Fig. 12A) is a measure of model uncertainty; the greater the distance the greater the uncertainty of the simulations.

- Another case is the existence of significant trends in the observations, but not in the simulations (Fig. 12C). In this situation, it is assumed that these trends as being due to non-climatic causes, which cannot be simulated by the models with stationary parameters. These non-climatic causes can be changes in land use, reforestation of agricultural fields, changes in infiltration due to human infrastructures, etcetera.
- There is a final situation, when the observed significant trends are simulated only by one of the models, either SWAT or SASER. In this case the situation is not easy to interpret. This situation is probably caused by differences in model structure. These are nonlinear models which may have many threshold effects. Thus, it may happen that one model starts exhibiting a trend earlier than the other one, depending on thresholds being surpassed.

Finally, it should be noted that both models used the same meteorological forcing. Thus, errors in the meteorological forcing are propagated to both models in an equal manner. If observed climate trends are not correctly reproduced by the forcing dataset, the models will not be able to simulate them.

Discussion and conclusions.

This study allowed to quantify the trends of streamflow statistics (low, medium and high flows) of Pyrenean rivers. It has been done both in observed and simulated time series, which have been computed using two very different hydrological models, with the aim of analyzing how models with fixed physiography and very different structure simulate trends in this area of study.

The first and most important result is that most of the time series did not present statistically significant trends over the period 1980–2013, probably due to the high variability of the climate of the region, which makes trend detection more difficult in such a

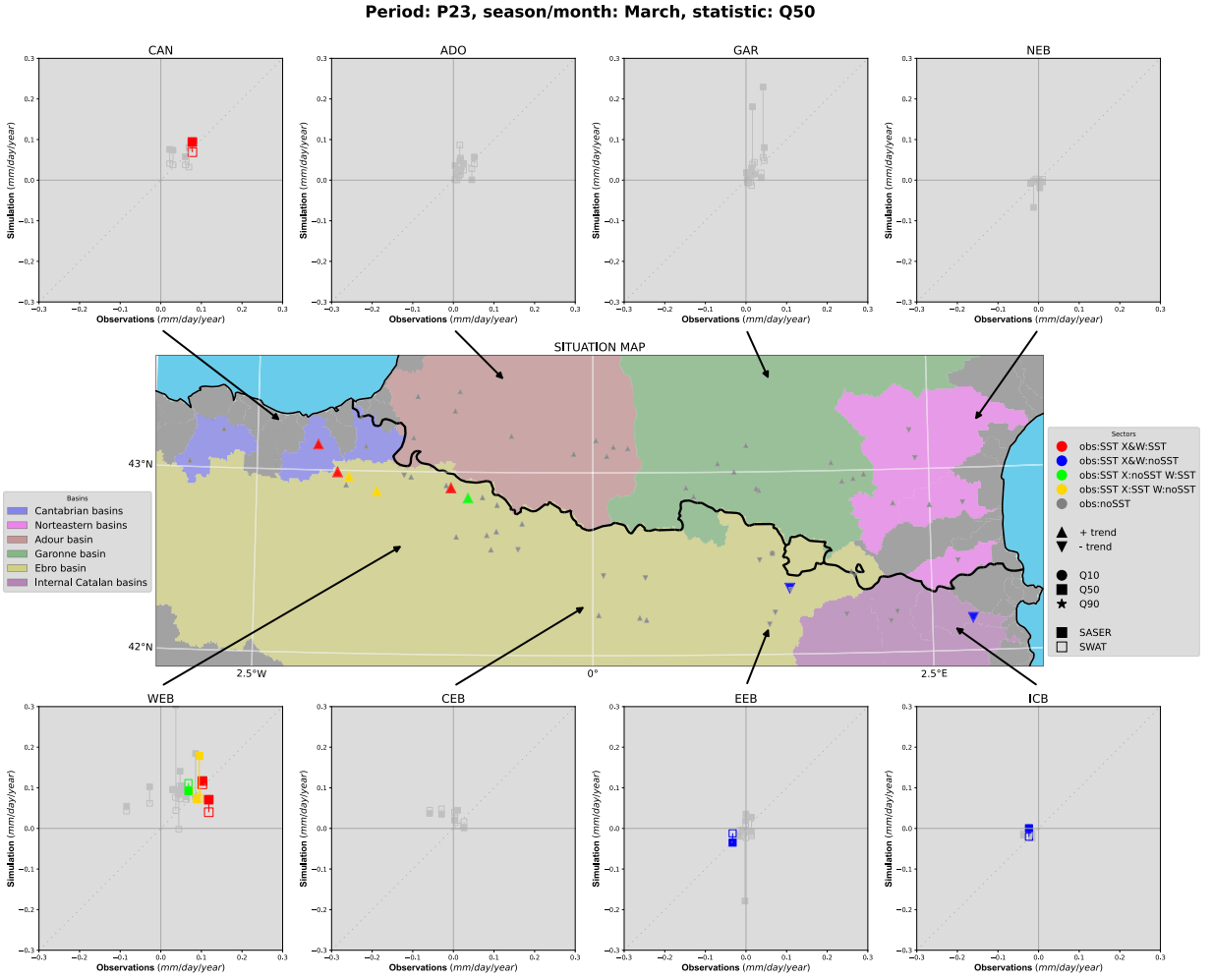

Fig. 10. Statistically significant trend distribution by regions in a map and their graphical representation for March, the Q50 percentile, and the 1990–2013 (P23). The positive significant trends (observed and simulated) sited in the western parts contrast with the negative observed significant trends (not simulated) in the southeastern regions.

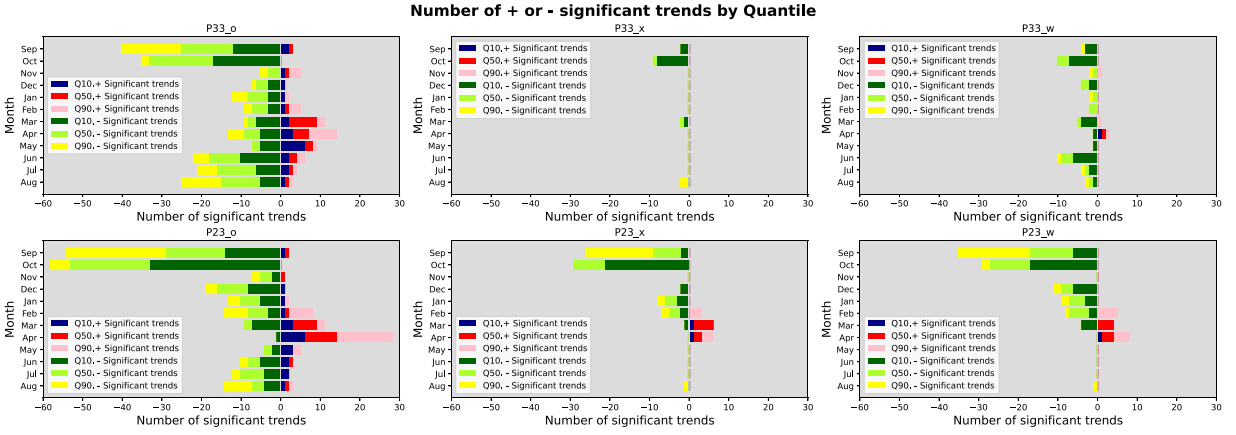

Fig. 11. Distributions of the significant trends by months. P33 is the period from 1980 to 2013 and P23 is the 1990–2013 period. The 'o' refers to observations, 'w' refers to the SWAT model, and 'x' refers to the SASER model. Each bar is the number of significant trends by quantile for each month, the negative values of the x-ticks refer to the number of negative significant trends.

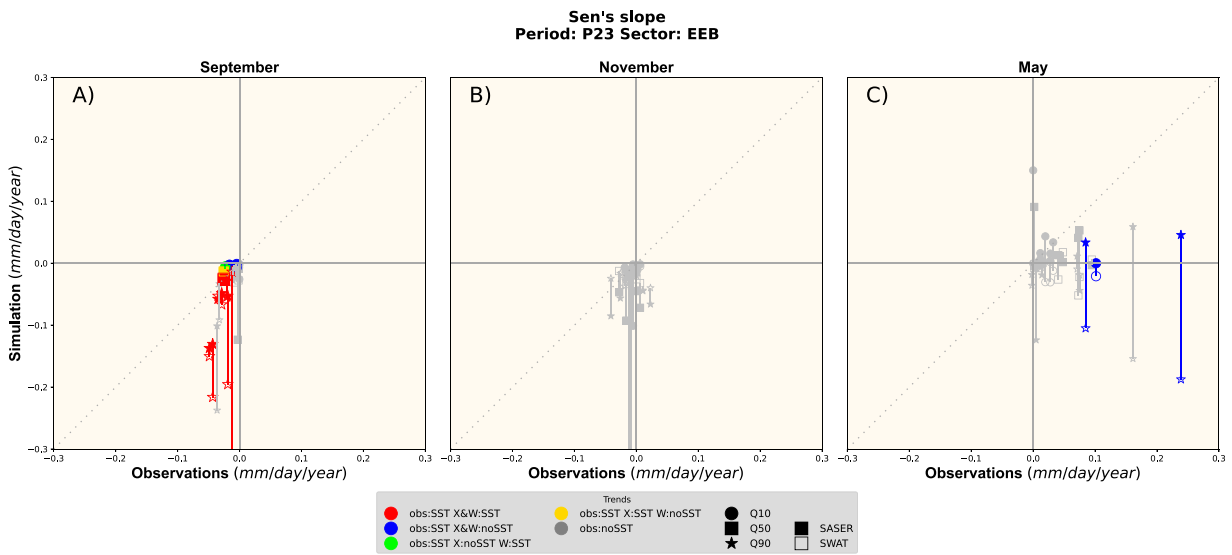

Fig. 12. Graphical representation of Sent trends by months. P33 is the period from 1980 to 2013 and P23 is the 1990–2013 period. The 'o' refers to observations, 'w' refers to the SWAT model, and 'x' refers to the SASER model. Each bar is the number of sianges in climate. B) November: None of the calculated trends is statistically significant (gray symbols). C) May: some of Q90 and Q10 observed trends are statistically significant and are not simulated by SASER and SWAT models (blue symbols). We attribute these trends to non-climatic changes in the system.

relatively short time span.

Then, observations and models do not always reproduce the same trends. The models do not show good skill in reproducing the observed trends. Interpreting these differences is not always easy. However, non-simulated observed trends can be attributed to the parameters which are considered constant in the models, mainly LULC, which was considered static in the two models. It is well known that the Pyrenees has undergone major changes in land-use and land-cover since the mid-20th century, changes that have continued during the current century although probably at a slower rate (Beguería et al., 2003; Buendia et al., 2016; Gallart and Llorens, 2004, 2003; López-Moreno et al., 2006; Vicente-Serrano et al., 2021). These changes are mostly due to the abandonment of non-mechanizable or not very productive agricultural fields on the slopes of the Pyrenees. The abandoned lands have been artificially or naturally forested, leading to an increase in rainfall interception and evapotranspiration, among other changes.

If trends are observed in both simulations and observations, they are mainly attributed to climate (natural variability and anthropic causes), without ruling out other sources that may affect the magnitude of the simulated trends. Autumn is the season more affected by trends in the climate forcing, showing negative significant trends in the simulated and observed stream flows throughout the Pyrenees, especially affecting low flows (Q10). This pattern is even more marked in the southeastern part, which maintains this negative trend during winter. On the other hand, the positive significant trends are located in the western part of the Pyrenees at the end of winter (in high flows - Q90) and beginning of spring (in median flows - Q50), where, without ruling out other factors, a higher proportion of precipitation in liquid form and the earlier melting period have played an important role. Therefore, both seasonal and regional changes of natural river flows are seen.

Comparing the two time periods, 1980–2013 and 1990–2013, and looking at the Pyrenees as a whole, the number of observed time series with significant trends is similar in both periods, but it stands out that the models show more significant trends for the short period than for the long one. This raises the question of whether this means that the condition of a monotonic trend necessary for the MK test is not satisfied, which could be a limitation of the method.

As discussed above, the fact that the simulations do not give significant trends although the observations do, could be attributed to a set of parameters that are considered constant in the simulations, those related to land cover. Therefore, the differences between the two time periods are attributed to the fact that changes in land use and land cover have influenced flows more notably during the first decade than during the rest of the simulated time period and may be more remarkable than the effects of climate trends on Pyrenean River flows during this period.

The results show that the Mediterranean areas, which are more arid, are reducing their water flows and this process is accelerating, as shown by the comparison between the 1980–2013 and 1990–2013 periods. The progressive change to wetter conditions in the western and northern part of the domain is less affected by the streamflow decrease. Another conclusion is that, when trends are present, they often affect all percentiles. However, low flow trends tend to be stronger than higher flow trends.

Finally, the combination of climatic and non-climatic causes in a complex geographical domain and climatically diverse as the Pyrenees and with a not very long time series (33 years) gives large differences between the results of the models, revealing a large uncertainty and can complicate their interpretation. Using different models to properly quantify such uncertainties was a good choice. Studies based on a single model omit all these differences and can give a false sense of security. The two models are robust, common in the scientific literature, and very different from each other. With the available data, it is not possible to say which model reproduces the

overall water cycle best. Certainly, SWAT produces the best streamflow series, but it had to be expected since it was calibrated for that. In any case, both models are severely limited due to their fixed in time physiography and thus it has been shownus that there is a clear need to work towards future models that correctly reflect the actual evolution of the physiography. This is essential if stakeholders want to base future decision on past data.

CRediT authorship contribution statement

Roger Clavera-Gispert: Conceptualization, Methodology, Formal analysis, Investigation, Writing – original draft, Visualization. **Pere Quintana-Seguí**: Conceptualization, Methodology, Investigation, Resources, Data curation, Writing – review & editing, Supervision. **Leticia Palazón:** Resources, Data curation. **Ane Zabaleta:** Resources, Data curation. **Omar Cenobio:** Software, Validation, Investigation. **Anaïs Barella-Ortiz:** Software, Validation, Investigation, Writing – review & editing. **Santiago Beguería:** Conceptualization, Resources, Data curation, Writing – review & editing, Supervision, Project administration, Funding acquisition.

Declaration of Competing Interest

The authors declare that they have no known competing financial interests or personal relationships that could have appeared to influence the work reported in this paper.

Data Availability

The links and DOE of data are in the manuscript.

Acknowledgements

This work was supported by the project EFA210/16/PIRAGUA co-founded by the European Regional Development Fund (ERDF) through the Interreg V Spain-France-Andorre Programme (POCTEFA 2014-2020) of the European Union. The authors wish to thank the PIRAGUA team for their valuable work.

Appendix A. Supporting information

Supplementary data associated with this article can be found in the online version at doi:10.1016/j.ejrh.2023.101322.

References

Abbaspour, K.C., Johnson, C.A., van Genuchten, M.Th, 2004. Estimating Uncertain Flow and Transport Parameters Using a Sequential Uncertainty Fitting Procedure. Vadose Zone J. 3 (4), 1340–1352. https://doi.org/10.2113/3.4.1340.

Bayazit, M., 2015. Nonstationarity of hydrological records and recent trends in trend analysis: a state-of-the-art review. Environ. Process. 2 (3), 527–542. https://doi.org/10.1007/s40710-015-0081-7.

Beguería, S., López-Moreno, J.I., Lorente, A., Seeger, M., García-Ruiz, J.M., 2003. Assessing the effect of climate oscillations and land-use changes on streamflow in the central Spanish Pyrenees. Ambio 32 (4), 283–286. https://doi.org/10.1579/0044-7447-32.4.283.

Beguería, S., Palazón Tabuenca, L., Grusson, Y., Sánchez Pérez, J.M., Sauvage, S., Cakir, R., Quintana-Seguí, P., Barella, A., Vidal, J.-P., & POCTEFA-PIRAGUA Team. (2022). PIRAGUA_hydro_analysis [Dataset]. https://doi.org/10.20350/DIGITALCSIC/14667.

Bhuiyan, M.A.E., Nikolopoulos, E.I., Anagnostou, E.N., Quintana-Seguí, P., Barella-Ortiz, A., 2018. A nonparametric statistical technique for combining global precipitation datasets: development and hydrological evaluation over the Iberian Peninsula. Hydrol. Earth Syst. Sci. 22 (2), 1371–1389. https://doi.org/10.5194/hess-22-1371-2018.

Biancamaria, S., Mballo, M., Le Moigne, P., Sánchez Pérez, J.M., Espitalier-Noël, G., Grusson, Y., Cakir, R., Häfliger, V., Barathieu, F., Trasmonte, M., Boone, A., Martin, E., Sauvage, S., 2019. Total water storage variability from GRACE mission and hydrological models for a 50,000 km2 temperate watershed: The Garonne River basin (France). J. Hydrol. Reg. Stud. 24, 100609 https://doi.org/10.1016/j.ejrh.2019.100609.

Boone, A., Masson, V., Meyers, T., Noilhan, J., 2000. The influence of the inclusion of soil freezing on simulations by a soil–vegetation–atmosphere transfer scheme. J. Appl. Meteorol. Climatol. 39 (9), 1544–1569. https://doi.org/10.1175/1520-0450(2000)039<1544:TIOTIO>2.0.CO;2.

Buendia, C., Batalla, R.J., Sabater, S., Palau, A., Marcé, R., 2016. Runoff trends driven by climate and afforestation in a Pyrenean Basin. Land Degrad. Dev. 27 (3), 823–838. https://doi.org/10.1002/ldr.2384.

Büttner, G., 2014. CORINE Land Cover and Land Cover Change Products. In: Manakos, En.I., Braun, M. (Eds.), Land Use and Land Cover Mapping in Europe: Practices & Trends (p. 55-74). Springer, Netherlands. https://doi.org/10.1007/978-94-007-7969-3_5.

Cakir, R., Raimonet, M., Sauvage, S., Paredes-Arquiola, J., Grusson, Y., Roset, L., Meaurio, M., Navarro, E., Sevilla-Callejo, M., Lechuga-Crespo, J.L., Gomiz Pascual, J. J., Bodoque, J.M., Sánchez-Pérez, J.M., 2020. Hydrological alteration index as an indicator of the calibration complexity of water quantity and quality modeling in the context of global change. Art. 1 Water 12 (1). https://doi.org/10.3390/w12010115.

Choudhary, R., Athira, P., 2021. Effect of root zone soil moisture on the SWAT model simulation of surface and subsurface hydrological fluxes. Environ. Earth Sci. 80 (18), 620. https://doi.org/10.1007/s12665-021-09912-z.

Collaud Coen, M., Andrews, E., Bigi, A., Martucci, G., Romanens, G., Vogt, F.P.A., Vuilleumier, L., 2020. Effects of the prewhitening method, the time granularity, and the time segmentation on the Mann–Kendall trend detection and the associated Sen's slope. Atmos. Meas. Tech. 13 (12), 6945–6964. https://doi.org/10.5194/amt-13-6945-2020.

Cui, J., Zhao, Y., Sun, W., Chen, Y., Wu, B., Xue, B., Chen, H., Li, Z., Tian, Z., 2021. Evaluating the influence of hydrological condition on the phosphorus loads in an agricultural river basin using the SWAT model. Hydrol. Res. 52 (5), 1143–1158. https://doi.org/10.2166/nh.2021.165.

Datok, P., Sauvage, S., Fabre, C., Laraque, A., Ouillon, S., Moukandi N'kaya, G., Sanchez-Perez, J.-M., 2021. Sediment Balance Estimation of the 'Cuvette Centrale' of the Congo River Basin Using the SWAT Hydrological Model. Art. 10 Water 13 (10). https://doi.org/10.3390/w13101388.

David, Cédric H (2013). RAPID v1.4.0 (v1.4.0). Zenodo. https://doi.org/10.5281/ZENODO.24756.
David, C.H., Habets, F., Maidment, D.R., Yang, Z.-L., 2011. RAPID applied to the SIM-France model. Hydrol. Process. 25 (22), 3412–3425. https://doi.org/10.1002/hyp.8070.
Douglas-Mankin, K.R., Srinivasan, R., Arnold, J.G., 2010. Soil and water assessment tool (SWAT) model: current developments and applications. Trans. ASABE 53 (5), 1423–1431.
Durand, Y., Brun, E., Merindol, L., Guyomarc'h, G., Lesaffre, B., Martin, E., 1993. A meteorological estimation of relevant parameters for snow models. Ann. Glaciol. 18, 65–71. https://doi.org/10.3189/S0260305500011277.
Durand, Y., Giraud, G., Brun, E., Mérindol, L., Martin, E., 1999. A computer-based system simulating snowpack structures as a tool for regional avalanche forecasting. J. Glaciol. 45 (151), 469–484. https://doi.org/10.3189/S0022143000001337.
Earth Resources Observation And Science (EROS) Center, 2017. Global 30 Arc-Second Elevation (GTOPO30). [Work]. U.S. Geological Survey. https://doi.org/10.5066/f7df6pqs.
Faroux, S., Kaptué Tchuenté, A.T., Roujean, J.-L., Masson, V., Martin, E., Le Moigne, P., 2013. ECOCLIMAP-II/Europe: a twofold database of ecosystems and surface parameters at 1 km resolution based on satellite information for use in land surface, meteorological and climate models. Geosci. Model Dev. 6 (2), 563–582. https://doi.org/10.5194/gmd-6-563-2013.
Flipo, N., Monteil, C., Poulin, M., de Fouquet, C., Krimissa, M., 2012. Hybrid fitting of a hydrosystem model: long-term insight into the Beauce aquifer functioning (France). Water Resour. Res. 48 (5) https://doi.org/10.1029/2011WR011092.
Gallart, F., Llorens, P., 2003. Catchment management under environmental change: impact of land cover change on water resources. Water Int. 28 (3), 334–340. https://doi.org/10.1080/02508060308691707.
Gaona, J., Quintana-Seguí, P., Escorihuela, M.J., Boone, A., Llasat, M.C., 2022. Interactions between precipitation, evapotranspiration and soil moisture-based indices to characterize drought with high-resolution remote sensing and land-surface model data. Nat. Hazards Earth Syst. Sci. Discuss. 1–30. https://doi.org/10.5194/nhess-2022-65.
García-Ruiz, J.M., Beguería, S., López-Moreno, J.I., Lorente, A., Seeger, M.A., 2001. Los recursos hídricos superficiales del Pirineo aragonés y su evolución reciente. Geoforma Ediciones.
Grusson, Y., Sun, X., Gascoin, S., Sauvage, S., Raghavan, S., Anctil, F., Sáchez-Pérez, J.-M., 2015. Assessing the capability of the SWAT model to simulate snow, snow melt and streamflow dynamics over an alpine watershed. J. Hydrol. 531, 574–588. https://doi.org/10.1016/j.jhydrol.2015.10.070.
Grusson, Y., Anctil, F., Sauvage, S., Sánchez Pérez, J.M., 2017a. Testing the SWAT model with gridded weather data of different spatial resolutions. Art. 1 Water 9 (1). https://doi.org/10.3390/w9010054.
Grusson, Y., Anctil, F., Sauvage, S., Sánchez Pérez, J.M., 2017b. Assessing the climatic and temporal transposability of the SWAT model across a large contrasted watershed. J. Hydrol. Eng. 22 (6), 04017004. https://doi.org/10.1061/(ASCE)HE.1943-5584.0001491.
Grusson, Y., Anctil, F., Sauvage, S., Sánchez Pérez, J.M., 2018. Coevolution of hydrological cycle components under climate change: the case of the garonne River in France. Art. 12 Water 10 (12). https://doi.org/10.3390/w10121870.
Guinaldo, T., Munier, S., Le Moigne, P., Boone, A., Decharme, B., Choulga, M., Leroux, D.J., 2021. Parametrization of a lake water dynamics model MLake in the ISBA-CTRIP land surface system (SURFEX v8.1). Geosci. Model Dev. 14 (3), 1309–1344. https://doi.org/10.5194/gmd-14-1309-2021.
Habets, F., Boone, A., Noilhan, J., 2003. Simulation of a Scandinavian basin using the diffusion transfer version of ISBA. Glob. Planet. Change 38 (1), 137–149. https://doi.org/10.1016/S0921-8181(03)00016-X.
Hallouin, T. (2021). hydroeval: An evaluator for streamflow time series in Python [Python]. Zenodo. https://doi.org/10.5281/zenodo.4709652.
Hersbach, H., Bell, B., Berrisford, P., Biavati, G., Horányi, A., Muñoz Sabater, J., Nicolas, J., Peubey, C., Radu, R., Schepers, D., Simmons, A., Soci, C., Dee, D., Thépaut, J.-N., Rozum, I., 2018. ERA5 hourly data on single levels from 1979 to present. Copernicus Climate Change Service (C3S) Climate Data Store (CDS).
Jarvis, A., Reuter, H.I., Nelson, A., Guevara, A. (2008). Hole-filled SRTM for the globe Version 4 [Map]. ⟨https://cgiarcsi.community/data/srtm-90m-digital-elevation-database-v4–1/⟩.
Kaptue Tchuente, A.T., Roujean, J.-L., Faroux, S., 2010. ECOCLIMAP-II: an ecosystem classification and land surface parameters database of Western Africa at 1km resolution for the African Monsoon Multidisciplinary Analysis (AMMA) project. Remote Sens. Environ. 114 (5), 961–976. https://doi.org/10.1016/j.rse.2009.12.008.
Knoben, W.J.M., Freer, J.E., Woods, R.A., 2019. Technical note: inherent benchmark or not? Comparing Nash–Sutcliffe and Kling–Gupta efficiency scores. Hydrol. Earth Syst. Sci. 23 (10), 4323–4331. https://doi.org/10.5194/hess-23-4323-2019.
Labrousse, C., Ludwig, W., Pinel, S., Sadaoui, M., Lacquement, G., 2020. Unravelling climate and anthropogenic forcings on the evolution of surface water resources in Southern France. Art. 12 Water 12 (12). https://doi.org/10.3390/w12123581.
Lasanta, T., Nadal-Romero, E., Khorchani, M., Romero-Díaz, A., 2021. Una revisión sobre las tierras abandonadas en España: De los paisajes locales a las estrategias globales de gestión. Cuad. De. Invest. Geográfica 47 (2), 477–521. https://doi.org/10.18172/cig.4755.
Le Moigne, P., Besson, F., Martin, E., Boé, J., Boone, A., Decharme, B., Etchevers, P., Faroux, S., Habets, F., Lafaysse, M., Leroux, D., Rousset-Regimbeau, F., 2020. The latest improvements with SURFEX v8.0 of the Safran–Isba–Modcou hydrometeorological model for France. Geosci. Model Dev. 13 (9), 3925–3946. https://doi.org/10.5194/gmd-13-3925-2020.
Le Treut, H. (2013). Les impacts du changement climatique en Aquitaine: Un état des lieux scientifique. Presses universitaires de Bordeaux LGPA-éd.
Lehner, B., Verdin, K., Jarvis, A., 2008. New global hydrography derived from spaceborne elevation data. Eos Trans. Am. Geophys. Union 89 (10), 93–94. https://doi.org/10.1029/2008EO100001.
Lemus-Canovas, M., Lopez-Bustins, J.A., Trapero, L., Martin-Vide, J., 2019. Combining circulation weather types and daily precipitation modelling to derive climatic precipitation regions in the Pyrenees. Atmos. Res. 220, 181–193. https://doi.org/10.1016/j.atmosres.2019.01.018.
Lespinas, F., Ludwig, W., Heussner, S., 2010. Impact of recent climate change on the hydrology of coastal Mediterranean rivers in Southern France. Clim. Change 99 (3), 425–456. https://doi.org/10.1007/s10584-009-9668-1.
López-Moreno, J.I., Beguería, S., García-Ruiz, J.M., 2006. Trends in high flows in the central Spanish Pyrenees: Response to climatic factors or to land-use change? Hydrol. Sci. J. 51 (6), 1039–1050. https://doi.org/10.1623/hysj.51.6.1039.
López-Moreno, J.I., Vicente-Serrano, S.M., Moran-Tejeda, E., Zabalza, J., Lorenzo-Lacruz, J., García-Ruiz, J.M., 2011. Impact of climate evolution and land use changes on water yield in the ebro basin. Hydrol. Earth Syst. Sci. 15 (1), 311–322. https://doi.org/10.5194/hess-15-311-2011.
López-Moreno, J.I., Soubeyroux, J.-M., Gascoin, S., Alonso-Gonzalez, E., Durán-Gómez, N., 2020. Long-term trends (1958–2017) in snow cover duration and depth in the Pyrenees. Int. J. Climatol. 40 (14), 6122–6136. https://doi.org/10.1002/joc.6571.
Mann, H.B., 1945. Nonparametric tests against trend. Econometrica 13 (3), 245–259. https://doi.org/10.2307/1907187.
Martin, E., Gascoin, S., Grusson, Y., Murgue, C., Bardeau, M., Anctil, F., Ferrant, S., Lardy, R., Le Moigne, P., Leenhardt, D., Rivalland, V., Pérez, J.-M.S., Sauvage, S., Therond, O., 2016. On the Use of Hydrological Models and Satellite Data to Study the Water Budget of River Basins Affected by Human Activities: Examples from the Garonne Basin of France. In: Cazenave, En.A., Champollion, N., Benveniste, J., Chen, J. (Eds.), Remote Sensing and Water Resources. Springer International Publishing, pp. 33–57. https://doi.org/10.1007/978-3-319-32449-4_3.
Masson, V., Le Moigne, P., Martin, E., Faroux, S., Alias, A., Alkama, R., Belamari, S., Barbu, A., Boone, A., Bouyssel, F., Brousseau, P., Brun, E., Calvet, J.-C., Carrer, D., Decharme, B., Delire, C., Donier, S., Essaouini, K., Gibelin, A.-L., Voldoire, A., 2013. The SURFEXv7.2 land and ocean surface platform for coupled or offline simulation of earth surface variables and fluxes. Geosci. Model Dev. 6 (4), 929–960. https://doi.org/10.5194/gmd-6-929-2013.
Merheb, M., Moussa, R., Abdallah, C., Colin, F., Perrin, C., Baghdadi, N., 2016. Hydrological response characteristics of Mediterranean catchments at different time scales: A meta-analysis. Hydrol. Sci. J. 61 (14), 2520–2539. https://doi.org/10.1080/02626667.2016.1140174.
Morán-Tejeda, E., López-Moreno, J.I., Sanmiguel-Vallelado, A., 2017. Changes in Climate, Snow and Water Resources in the Spanish Pyrenees: Observations and Projections in a Warming Climate. In: Catalan, En.J., Ninot, J.M., Aniz, M.M. (Eds.), High Mountain Conservation in a Changing World. Springer International Publishing, pp. 305–323. https://doi.org/10.1007/978-3-319-55982-7_13.
Moucha, A., Hanich, L., Gascoin, S., Jarlan, L., 2020. Spatialization of meteorological variables over south mediterranean catchments. Case Tensift (Moroc.) 21910.

Noilhan, J., Mahfouf, J.-F., 1996. The ISBA land surface parameterisation scheme. Glob. Planet. Change 13 (1), 145–159. https://doi.org/10.1016/0921-8181(95)00043-7.

Noilhan, J., Planton, S., 1989. A simple parameterization of land surface processes for meteorological models. Mon. Weather Rev. 117 (3), 536–549. https://doi.org/10.1175/1520-0493(1989)117<0536:ASPOLS>2.0.CO;2.

Olaoye, I.A., Confesor, R.B., Ortiz, J.D., 2021. Impact of seasonal variation in climate on water quality of old woman creek watershed Ohio using SWAT. Art. 3 Climate 9 (3). https://doi.org/10.3390/cli9030050.

Pérez-Zanón, N., Sigró, J., Ashcroft, L., 2017. Temperature and precipitation regional climate series over the central Pyrenees during 1910–2013. Int. J. Climatol. 37 (4), 1922–1937. https://doi.org/10.1002/joc.4823.

Pool, S., Vis, M., Seibert, J., 2018. Evaluating model performance: towards a non-parametric variant of the Kling-Gupta efficiency. Hydrol. Sci. J. 63 (13–14), 1941–1953. https://doi.org/10.1080/02626667.2018.1552002.

Quintana-Seguí, P. (2022). PIRAGUA_atmos_analysis [Dataset]. https://doi.org/10.20350/DIGITALCSIC/14665.

Quintana-Seguí, P., Moigne, P.L., Durand, Y., Martin, E., Habets, F., Baillon, M., Canellas, C., Franchisteguy, L., Morel, S., 2008. Analysis of near-surface atmospheric variables: validation of the SAFRAN analysis over France. J. Appl. Meteorol. Climatol. 47 (1), 92–107. https://doi.org/10.1175/2007JAMC1636.1.

Quintana-Seguí, P., Peral-García, M.C., Turco, M., Llasat, M.C., Martin, E., 2016. Meteorological analysis systems in North-East Spain: validation of SAFRAN and SPAN. J. Environ. Inform. 27, 116–130. https://doi.org/10.3808/jei.201600335.

Quintana-Seguí, P., Turco, M., Herrera, S., Miguez-Macho, G., 2017. Validation of a new SAFRAN-based gridded precipitation product for Spain and comparisons to Spain02 and ERA-Interim. Hydrol. Earth Syst. Sci. 21 (4), 2187–2201. https://doi.org/10.5194/hess-21-2187-2017.

Quintana-Seguí, P., Barella-Ortiz, A., Regueiro-Sanfiz, S., Miguez-Macho, G., 2020. The utility of land-surface model simulations to provide drought information in a water management context using global and local forcing datasets. Water Resour. Manag. 34 (7), 2135–2156. https://doi.org/10.1007/s11269-018-2160-9.

Quintana-Seguí, P., Caballero, Y., Cakir, R., Dewandel, B., Grusson, Y., Jódar, J., Lambán, J.L., Lanini, S., Cointe, P.L., Llasat, M. del C., Sánchez-Pérez, J.M., Sauvage, S., Palazón, L., Zabaleta, A., Beguería, S. (2021). Comparison and validation of the Pyrenean hydrological cycle simulated by different modeling approaches using in-situ and remote sensing data. (Núm. EGU21–4675). EGU21. Copernicus Meetings. ⟨https://doi.org/10.5194/egusphere-egu21–4675⟩.

Saleh, F., Flipo, N., Habets, F., Ducharne, A., Oudin, L., Viennot, P., Ledoux, E., 2011. Modeling the impact of in-stream water level fluctuations on stream-aquifer interactions at the regional scale. J. Hydrol. 400 (3), 490–500. https://doi.org/10.1016/j.jhydrol.2011.02.001.

Sen, P.K., 1968. Estimates of the regression coefficient based on Kendall's Tau. J. Am. Stat. Assoc. 63 (324), 1379–1389. https://doi.org/10.1080/01621459.1968.10480934.

Stahl, K., Hisdal, H., Hannaford, J., Tallaksen, L.M., van Lanen, H.A.J., Sauquet, E., Demuth, S., Fendekova, M., Jódar, J., 2010. Streamflow trends in Europe: Evidence from a dataset of near-natural catchments. Hydrol. Earth Syst. Sci. 14 (12), 2367–2382. https://doi.org/10.5194/hess-14-2367-2010.

Tóth, H., Szintai, B., 2021. Assimilation of leaf area index and soil water index from satellite observations in a land surface model in hungary. Art. 8 Atmosphere 12 (8). https://doi.org/10.3390/atmos12080944.

Tramblay, Y., Feki, H., Quintana-Seguí, P., Guijarro, J.A., 2019. The SAFRAN daily gridded precipitation product in Tunisia (1979–2015). Int. J. Climatol. 39 (15), 5830–5838. https://doi.org/10.1002/joc.6181.

Vicente-Serrano, S.M., López-Moreno, J.I., 2006. The influence of atmospheric circulation at different spatial scales on winter drought variability through a semi-arid climatic gradient in Northeast Spain. Int. J. Climatol. 26 (11), 1427–1453. https://doi.org/10.1002/joc.1387.

Vicente-Serrano, S.M., Domínguez-Castro, F., Murphy, C., Peña-Angulo, D., Tomas-Burguera, M., Noguera, I., López-Moreno, J.I., Juez, C., Grainger, S., Eklundh, L., Conradt, T., Azorin-Molina, C., El Kenawy, A., 2021. Increased vegetation in mountainous headwaters amplifies water stress during dry periods. e2021GL094672 Geophys. Res. Lett. 48 (18). https://doi.org/10.1029/2021GL094672.

Vidal, J.-P., Martin, E., Franchistéguy, L., Baillon, M., Soubeyroux, J.-M., 2010. A 50-year high-resolution atmospheric reanalysis over France with the Safran system. Int. J. Climatol. 30 (11), 1627–1644. https://doi.org/10.1002/joc.2003.

Vogt, F.P.A. (2021). mannkendall/Python: Bug fix: prob_mk_n (v1.1.0). Zenodo. https://doi.org/10.5281/ZENODO.4495590.

Vural, J., Schneider, S., Bauer-Marschallinger, B., Haslinger, K., 2021. Assimilation of the SCATSAR-SWI with SURFEX: impact of local observation errors in Austria. Mon. Weather Rev. 149 (3), 773–791. https://doi.org/10.1175/MWR-D-20-0160.1.

Wieder, W.R., Boehnert, J., Bonan, J.B., Langseth, M., 2014. Regridded harmonized world soil database v1.2. Oak Ridge Natl. Lab. Distrib. Act. Arch. Cent. https://doi.org/10.3334/ORNLDAAC/1247.

Yang, J., Reichert, P., Abbaspour, K.C., Xia, J., Yang, H., 2008. Comparing uncertainty analysis techniques for a SWAT application to the Chaohe Basin in China. J. Hydrol. 358 (1), 1–23. https://doi.org/10.1016/j.jhydrol.2008.05.012.

Zabaleta, A., Meaurio, M., Morales, T., Damas, L., 2019. Vulnerabilidad hídrica del Golfo de Bizkaia: De las tendencias del pasado reciente a las del futuro. Geogaceta 66, 55–58.

Zabaleta, A., Beguería, S., Antigüedad, I., Lambán, J., Hakoun, V., Jung, M., Le Cointe, P., & Caballero, Y. (2022). PIRAGUA_indicators [Dataset]. https://doi.org/10.20350/DIGITALCSIC/14658.